A push in the right direction: exploring the role of Zealandia collision in Eocene Pacific-Australia plate motion changes

Dan Sandiford[1,2], Peter Betts[1], Joanne Whittaker[3], Louis Moresi[4]

[1]Monash University
[2]University of Sydney
[3]University of Tasmania, Institute of Marine and Antarctic Studies
[4]Australian National University

Key Points:

- During the Eocene tectonic reorganization, the Pacific Plate rotation vector developed increased radial component (spin around the centroid)
- The geometry of both the Zealandia and IBM margins would have facilitated strong radial torque partitioning of plate boundary normal forces
- Global-scale numerical models support our geometric analysis, particularly in terms of the role of the Izu-Bonin-Marianas margin (IBM)

Corresponding author: Dan Sandiford, dansandifordscience@gmail.com

Abstract

The Pacific Plate underwent a significant change in motion during the early Eocene. This change has been linked to plate boundary reconfiguration, particularly in relation to subduction margins. The reconfiguration also resulted in a new Pacific-Australian plate boundary section transecting Zealandia. Following the Eocene transition, the relative rotation axis was located within continental Zealandia, and it has been hypothesized that this region acted as a pivot point. Here we investigate the extent to which collision resistance along the intra-continental Zealandia margin (length ~ 1000 km) might have impacted the motion of the Pacific Plate, which is characterised by trench lengths more than an order of magnitude greater. We first highlight the relatively large radial component in the Pacific Plate absolute rotation during the period ca. 47-32 Ma (i.e. the spin around the plate centroid axis). We then consider how parameterised plate boundary forces impact the tangential and radial components of the net torque (i.e. the fictitious and true torque components). We show that during this period, both the Zealandia and Izu-Bonin-Marianas (IBM) margins of the Pacific Plate were well-oriented in terms of partitioning boundary normal forces into counter-clockwise (CCW) radial torques. This analysis is supported by results from recent global-scale numerical models. The role of Zealandia cannot be established unambiguously, based on our analysis, but effects can be quantified under different assumptions. Collision resistance along the Zealandia margin could plausibly constitute a 'first order' effect on Eocene Pacific Plate rotation, albeit only on the radial component.

1 Approach and context of study

This study is motivated by questions relating to the motion of the Pacific and Australian plates during the period of significant reorganisation of plate motions (ca. 50 Ma), which we refer to as the 'Eocene transition' (Whittaker et al., 2007). The change in Pacific Plate motion at this time is associated with the prominent bend in the Hawaii-Emperor Seamount Chain (Morgan, 1972; Hu et al., 2022b). Fig. 1 shows the tectonic configuration, before (57 Ma) and shortly after (47 Ma) the Eocene transition, where the westwards change in Pacific Plate motion can be identified in the orientation of velocity vectors. The change in absolute Pacific Plate motion has predominately been attributed to the evolution of subduction margins, including cessation of Izanagi Plate subduction and subduction of the Izanagi-Pacific Ridge, subduction initiation (e.g. the Izu-Bonin-Marianas, or IBM margin) and subduction polarity reversal (Whittaker et al., 2007; Wessel & Kroenke, 2008; Faccenna et al., 2012; Sutherland et al., 2017; Hu et al., 2022b). In particular, the initiation of the IBM margin has been identified as a key event (Sutherland et al., 2017; Hu et al., 2022b; Gurnis, 2023).

Along with changes in Pacific Plate subduction margins, the Eocene transition also involved reconfiguration of Pacific-Australian plate boundary as well as relative motion between these plates. Tasman Sea spreading ceased at about 50 Ma, and the Pacific-Australian plate boundary relocated onto a fault zone transecting the rifted Gondwanan fragment of Zealandia (Gaina et al., 1998). We refer to the intra-continental part of this boundary as the 'Zealandia margin', as shown in the upper right panel of Fig. 2. Although this fault zone is inferred to significantly predate the Eocene transition (Lamb et al., 2016), the critical change at this time was the transfer of Pacific-Australian relative motion onto this system.

During the period ca. 45-30 Ma (and potentially somewhat earlier) the Euler pole of relative rotation between the Pacific and Australian Plates, was situated within or close to Zealandia (Sutherland, 1995; Keller, 2005). Fig. 2b shows two relative Euler pole locations inferred at times near the Eocene transition. The black circle is the 47 Ma pole from Müller et al. (2016), and is derived from a plate circuit (relative motion model) through the West-Antarctic (W-ANT) and Antarctic (ANT) plates. The black cross is the 45 Ma

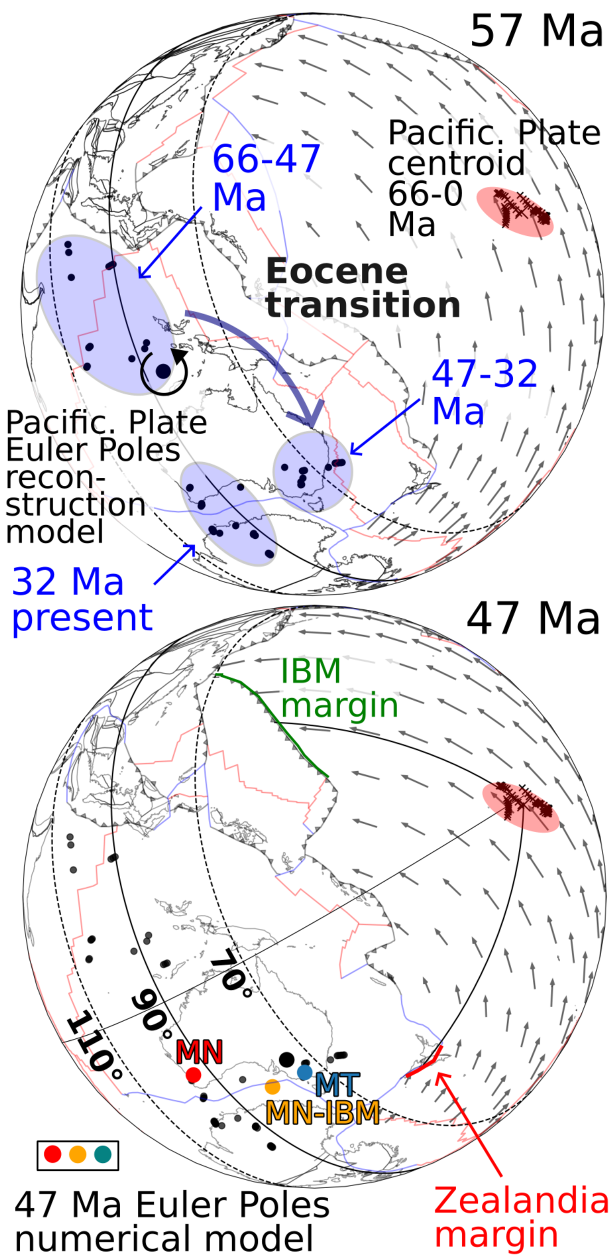

Figure 1. Tectonic configuration of the SW Pacific, shown before (57 Ma) and after (47 Ma) the Eocene transition. All tectonic features are based on the plate reconstruction model of Müller et al. (2016), with alternative north Pacific subduction margins as presented in Hu et al. (2022b). Cenozoic locations of Pacific Plate Euler poles are shown with black circles, from the same reconstruction models. The larger black circle shows the Euler pole at the reconstruction time; arrow shows the CCW rotation sense. Euler poles and plate velocity arrows reflect Pacific Plate rotations in the absolute reference frame described in Müller et al. (2016). A great circle at an angle of 90° to the Pacific Plate centroid is shown with a solid black line, as labelled. Three distinct clusters in Euler pole locations can be identified, as highlighted by blue regions and labels in the top panel. The Eocene transition (indicated by the blue arrow) corresponds to a migration of the Euler pole location towards the southeast, as well as a ∼ 25° migration towards the Pacific Plate centroid. Centroid locations at 1 Myr intervals throughout the Cenozoic are shown with black crosses, and highlighted in the red region. In the lower panel, the red, blue and yellow circles show Pacific Plate Euler poles from 3 global numerical models presented in Hu et al. (2022b).

Euler pole from Sutherland (1995), which is the earliest direct estimate of relative motion determined from spreading features in the Emerald Basin (the location of which is shown in the lower right panel of Fig. 2). The pole locates in central Zealandia, close to the inferred western limit of the underthrust Hikurangi Plateau (HP).

The Hikurangi Plateau is thought to play a central role in the evolution of Zealandia (Reyners, 2013; Mortimer, 2018). This region emerged as part of the Ontong-Java large igneous province at ca. 120 Ma (Mahoney et al., 1993), later colliding with the Gondwanan arc and underthrusting the continental margin. Back arc spreading commenced at around 90 Ma, leading to the opening of the Tasman Sea and the progressive rifting of Zealandia, including the underthrust HP, away from Gondwana (Gaina et al., 1998). This phase is shown in the upper left panel of Fig. 2. In relation to Pacific-Australian plate motion following the Eocene transition, Reyners (2013) has proposed that "resistance of the [Hikurangi] plateau to subduction had a first-order effect". In particular, "the western tip of the [Hikurangi] plateau appears to have acted as a pivot point on the plate boundary" (see also Eberhart-Phillips et al. (2018)).

In terms of the absolute motion of Pacific Plate, the Eocene transition comprised significant changes in, respectively, the tangential and radial components of the rotation vector (as we show in Section 2). Moreover, changes in both of these components facilitate an overall shift of absolute Pacific Plate Euler poles toward Zealandia. In this way, we highlight the potential connection between changes in absolute Pacific Plate motion, as well as its motion relative to the Australian Plate. In sections 3&4 we investigate the extent to which forces acting along the Zealandia margin could have impacted this change in (absolute) Pacific Plate motion. This represents an attempt to quantitatively evaluate the hypothesis of Reyners (2013). Specifically, we evaluate the relative effects of a putative collision resistance at the Zealandia margin, compared with Pacific Plate margin subduction forces. While this type of geometric analysis has an extensive history in the literature (Forsyth & Uyeda, 1975; Becker & O'Connell, 2001; Faccenna et al., 2012), the novelty here is to investigate how such margin-normal forces would contribute to what we describe as the tangential and radial components of the net torque.

The context and approach of our study is informed by the idea that while plates are driven/resisted by a range of mechanisms, not all of these are capable of evolving rapidly (Faccenna et al., 2012; Colli et al., 2014; Hu et al., 2022b). For instance, plates may be coupled to a whole-mantle flow through basal shear as well as forces due to dynamic topography (Steinberger et al., 2001). While such contributions are thought to play a significant role in terms of Cenozoic Pacific Plate dynamics, they are also expected to evolve slowly (Steinberger et al., 2001; Faccenna et al., 2012; Stotz et al., 2018). On the other hand, forces such as direct slab pull, and collision resistance, are viewed as being capable of evolving rapidly (England & Molnar, 2022; Hu et al., 2022b). The implication of these points is that torques due to subduction and collision represent only a partial description of the overall plate equilibrium. This has important implications for how we interpret comparisons between torques and plate rotation vectors. We pick up on this issue in Section 4. We will also address the limitations of our simple geometric analysis, by considering results from recent global-scale numerical models (Hu et al., 2022b).

2 Plate motion models

In this study we use a global plate reconstruction model (Müller et al., 2016) to address both the relative and absolute rotations of the Pacific and Australian plates. By absolute rotations, we are referring both to the model of relative motions as well as the reference frame to which the relative motion model is anchored. Following Müller et al. (2016), the relative motion model is fixed (for the past 100 Ma) to a global moving hotpot model (Torsvik et al., 2008). The evolution of Pacific Plate Euler poles in the Müller et al. (2016) model is shown in Fig. 1, while additional reference frames are shown in

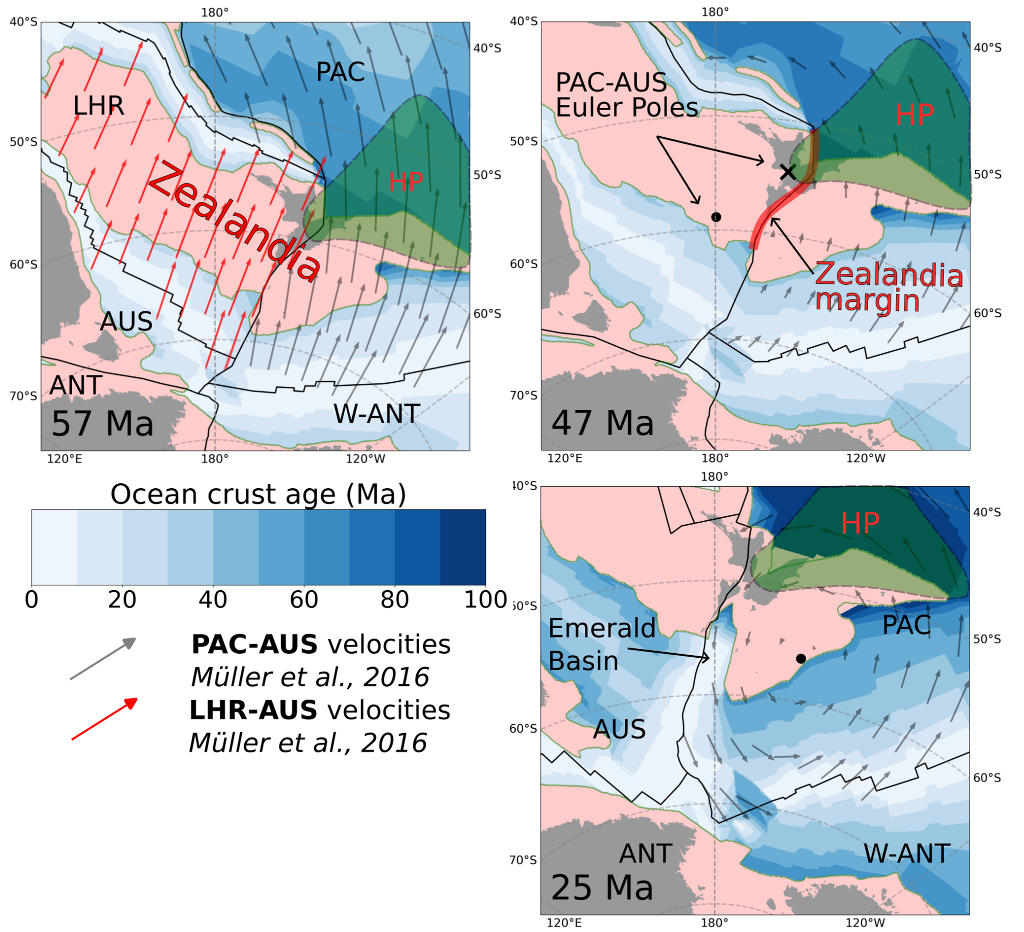

Figure 2. Cenozoic evolution of the Pacific-Australia plate boundary system based on the plate reconstruction of Müller et al. (2016); geometries are shown relative to the absolute reference frame. Pink regions represent approximate extents of continental crust; grey regions are reconstructions of current-day coastlines; green region is the approximate extent of the Hikurangi Plateau (HP), including the parts inferred to be underthrust beneath Zealandia (see Reyners (2013) for geophysical constraints). Solid black lines show plate boundaries from Müller et al. (2016). Black labels in the upper left panel are abbreviations for the plates, as discussed in the main text. The Zealandia margin – the intra-continental part of the Pacific-Australian plate boundary – is highlighted with red. The black velocity arrows show the rotation of the Pacific Plate relative to a stationary Australian Plate (red arrows show the same for the Lord Howe Rise Plate). In the top left panel (57 Ma) Zealandia straddles the Pacific and LHR plates, which are both rifting north from Gondwana, along with minor relative rotation. The Euler poles for Pacific-Australian relative motion, from Müller et al. (2016), are shown with the black circles. The black cross in the upper right is the 45 Ma Euler pole estimated by Sutherland (1995) from spreading features in the Emerald Basin. Lower right panel shows the incipient phase of Alpine Fault System.

Supplementary Fig. S1, including a fixed Pacific hotspot frame (Wessel & Kroenke, 2008). While the overall trajectories of these poles show significant similarity, there are non-trivial differences in timing. These differences are more obvious when we consider the decomposition of the rotation vectors at the plate centroid (as shown in Fig. S2, and discussed later in this Section). Since there appears to be general consensus for moving Pacific hotpots (Steinberger, 2000; Torsvik et al., 2008), our analysis focuses on absolute plate motions models based on global moving hotpot frames (Müller et al., 2016; Torsvik et al., 2008).

In terms of trying to quantify the role of tectonic forces in driving changes in plate motion, we focus primarily on the changes expressed in the absolute motion of Pacific Plate (for reasons that are elaborated throughout the manuscript). The Cenozoic absolute rotation poles of the Pacific Plate are shown with black circles in Fig. 1. Three distinct clusters in pole locations can be identified, as highlighted by blue regions and labels. An important observation, particularly in the context of this study, is that during the Eocene transition, Pacific Plate Euler poles shift much closer to Zealandia. This suggests that changes in the absolute motion of the Pacific Plate partly facilitated the corresponding change in the locations of the relative (Pacific-Australian) poles, such that the latter were located within or close to Zealandia throughout the pivot period. This relationship cannot simply be assumed at the outset, as the relative Euler poles could (in principle) be completely controlled by changes in the Australian Plate absolute motion. This does not seem to be the case. These connections also underpin our focus on Pacific Plate absolute motion throughout the remainder of the manuscript.

A key aspect of this study is to consider a decomposition of the plate rotations into 'radial' and 'tangential' components. The radial component is the spin around an axis ($\hat{r}_c$) that points radially outwards at the plate centroid. The decomposition of the plate rotation vector ($\vec{\omega}$) can simply be expressed as:

$$\begin{aligned} \vec{\omega}_{\mathrm{rad}} &= \vec{\omega} \cdot \hat{r}_c \\ \vec{\omega}_{\mathrm{tan}} &= \vec{\omega} - \vec{\omega}_{rad} \end{aligned} \tag{1}$$

Note that when a plate rotation is purely tangential (at the centroid), the rotation axis is orthogonal to the centroid vector, and hence the Euler pole of the rotation lies at 90° from the plate centroid; the finite rotation at the centroid is then a great circle arc. In contrast, the plate rotation is purely radial when the Euler pole lies at the plate centroid, in which case the plate spins about the radial axis.

The radial and tangential rotation components expressed in Eq. 1 will clearly depend on the magnitude of the rotation vector $\vec{\omega}$. However, if we consider only the orientation of $\vec{\omega}$, (i.e. $\hat{\omega}$), then the radial component of rotation can be approximated as an angle:

$$\hat{\omega}_{\mathrm{rad}} = \cos(\gamma) = \sin(\frac{\pi}{2} - \gamma) \approx (\frac{\pi}{2} - \gamma) \tag{2}$$

where γ is the angle between the Euler pole and the centroid, and the small angle approximation is made. This expression shows that the relative amount of plate radial rotation, has an intuitive geographic representation, being the angle between the Euler pole and a great circle drawn at 90° from the centroid. Supplementary Fig. S3 shows a comparison between the approximation of the radial component of Pacific Plate rotation ($\frac{\pi}{2} - \gamma$) and the true radial component ($\vec{\omega}_{\mathrm{rad}}$, in units of °/100 Ma). Note that with this choice of units, the magnitude of the Pacific Plate radial component, in both the true and approximate measure, are very similar.

Fig. 3 shows the Cenozoic evolution of Pacific Plate rotation, decomposed into radial and tangential components. The tangential component of the rotation has additionally been decomposed into an azimuth (Fig. 3A) and a magnitude (Fig. 3B) at the centroid. This decomposition shows that the Eocene transition (ca. 47 Ma) involved both the (often-discussed) westwards change in the rotation azimuth, as well as a significant (CCW) change in the radial rotation component (Fig. 3C). In fact, the period of 47-32 Ma is associated with the largest Pacific Plate radial rotation component of any time during the Cenozoic. This period of higher radial rotation overlaps broadly the same interval (ca. 45-30 Ma) where estimates of Pacific-Australian relative motion place the rotation pole within Zealandia (Sutherland, 1995). Based on this association, we refer to this interval as the 'pivot period'. Following this period, the (absolute) Pacific Plate radial rotation component rapidly reverted to weakly CW, and remained relatively stable until about 10 Ma, when a further $\sim 5^\circ$ (CW) increase occurred. In the following section we analyse how plate boundary normal forces contribute to the torque components that may drive such changes in plate rotation. This begins with a general development, which is then applied to Pacific Plate margins in the Cenozoic.

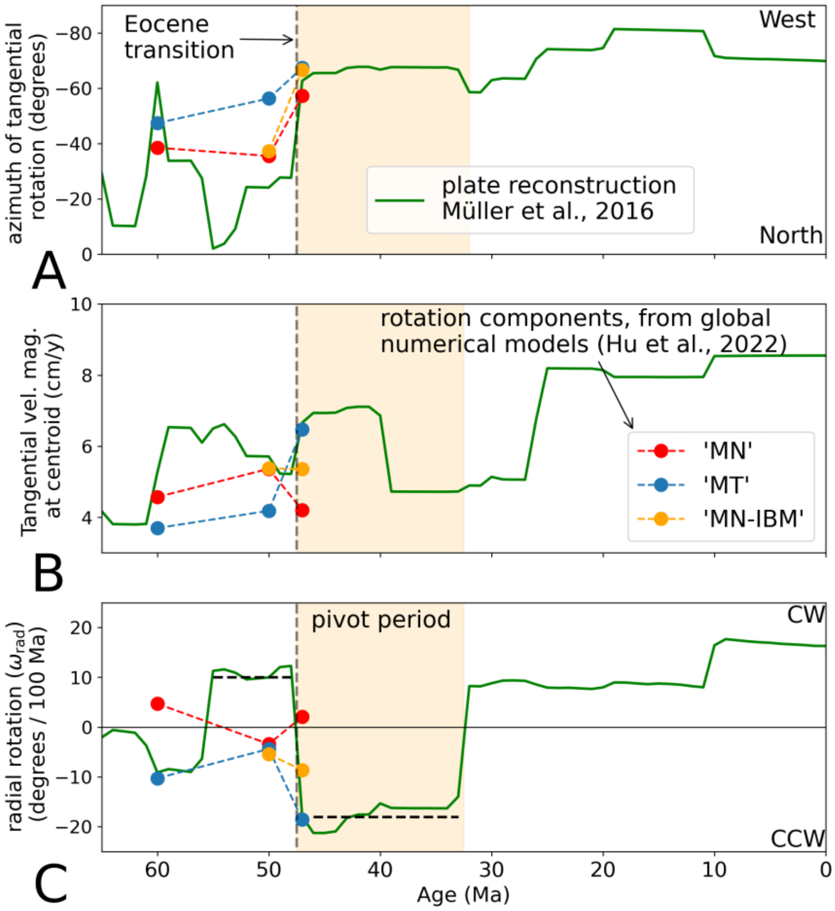

Figure 3. Cenozoic Pacific Plate motion trends, relative to hotspot reference frames, evaluated at the Pacific Plate centroid, based on plate reconstruction model if (Müller et al., 2016). As discussed in the main text, the Figure shows a decomposition of the plate rotation vector into: A) the azimuth of the velocity at the centroid; B) the magnitude of the tangential part of the rotation vector; and C) the radial rotation component. In this study, the Eocene transition is defined as the time associated with the significant (westwards) azimuthal change in Pacific Plate motion. In the plate reconstructions analysed in this study, the Eocene transition occurs at 47 Ma, although a window of at least several million years is suggested by previous studies (Whittaker et al., 2007; O'Connor et al., 2015). The 'pivot period' (ca. 47 - 32 Ma) is defined as the duration of relatively strong CCW radial rotation on the Pacific Plate; this interval largely coincides with the period in which the relative Pacific-Australian Euler poles were located within or close to Zealandia. The colored circles show Pacific Plate rotation components, as predicted in global-scale numerical models (Hu et al., 2022b). These numerical model results are discussed in Section 5.

3 Theory and methods

3.1 Torques due to plate boundary force

Because plate motion is restricted to the surface of a sphere, the 6 degrees of freedom that apply to rigid body motion, can be reduced to 3 rotational components (Forsyth & Uyeda, 1975; Bird et al., 2008). The equilibrium problem is then to understand the balance of torques that give rise to observed rotations. For plate motions, rotations are commonly expressed in terms of a rotation axis (or Euler pole) and angular velocity, or simply a rotation vector ($\vec{\omega}$).

The rotations and torques are naturally described with respect to the center of the Earth, and hence the radius of the Earth enters the description as the moment arm length. For instance, in terms of parameterised plate boundary forces (Forsyth & Uyeda, 1975; Becker & O'Connell, 2001), the torque vector component due to a plate boundary normal force, over a small section of trench, may be written as:

$$d\vec{\tau} = F_n(\vec{r_0} \times \hat{n})dl \tag{3}$$

Where F_n is the (scalar) normal force density (force per unit length, expressed in this study in units of TN/m), $\hat{n}$ is a unit vector in the local tangent plane that is normal to the plate boundary, and $\vec{r_0}$ is the radius vector that points to the location of the plate boundary. The total torque due to plate boundary normal forces is:

$$\vec{\tau}_{\text{net}} = \sum F_n(\vec{r_0} \times \hat{n})dl \tag{4}$$

Eq. 4 represents a typical description used to investigate mechanical equilibrium of rigid plates on a sphere (Forsyth & Uyeda, 1975; Becker & O'Connell, 2001). However, this description tends to obscure an important aspect of the mechanics, which is that the torque vector described by Eqs. 3 and 4, conflates two kinds of torques. The distinction between these types of torques is closely related to the more familiar case of the motion of a solid object constrained to a planar surface. The mechanical descriptions converge for very small plates, which are approximately planar. Fig. 4 attempts to clarify these relationships. We will hereafter condense the notation by denoting the point force along a small boundary increment (dl) as $\vec{F_n} = F_n dl\, \hat{n}$, and dropping the differential symbol, so that Eq. 3 can be written as:

$$\vec{\tau} = \vec{r_0} \times \vec{F_n} \tag{5}$$

Fig. 4 shows the effect of an arbitrary point force $\vec{F_n}$ acting on a square plate confined to (a) a planar surface and (b) the surface of a sphere. Note that in both cases the z axis is aligned with the vertical direction at the centroid of the plate. The line that connects the centroid to the point force location, is referred to as the centroid direction. The centroid directions are shown with the solid blue line in (a) and the solid blue arc in (b). Note that the centroid direction is parallel to the y axis (in a) and lies in the y-z plane (in b). In the latter case, 'parallel to the centroid direction', means parallel to the local orientation of the centroid direction arc, i.e. a vector in the local tangent plane.

In each case a point force, represented by a green arrow, acts at the corner of the square plate. This point force is parallel to the direction given by the dashed edge, and hence normal to the adjacent edge. The point force vector has been decomposed into components that are parallel (blue) and orthogonal (brown) to the centroid direction. In the planar case (a), a torque arises because the point force (green vector) has a component that is orthogonal centroid direction; this orthogonal component of the point force is given by $|\vec{F}_n|\sin(\theta)$, and the torque is given by $\vec{r}\times\vec{F}_n$, or $-|\vec{F}_n||\vec{r}|sin(\theta)\hat{z}$. However this orthogonal component also contributes to the net (linear) force on the plate. We use the brown arrow to signify the contribution (of the orthogonal component of the point force) to the linear force, and the black arrow to signify the contribution to the torque.

Now we consider the extension of this behavior to the spherical case. In the conventional analysis of plate boundary forces, a point force $\vec{F}_n$, such as is shown with the green arrow in (b), will be assumed to contribute to a driving torque τ (as in Eqs. 3 or 5). Similar to the foregoing analysis, we can decompose this torque in such a way as to highlight the contributions of the force components that act parallel and orthogonal to the centroid direction.

Consider first the component of the torque associated with the force parallel to the centroid direction (blue arrow). For the configuration shown in (b), this component of the torque vector is parallel to the x axis. The moment arm length is r_0, it has no dependence on the location of the point force (which is analogous to the planar case). This component of the driving torque produces purely tangential motion at the centroid, because $\hat{r}_c\times\hat{x}$ is tangent to the surface, where $\hat{r}_c$ is a unit vector that points radially outward at the centroid. For the configuration shown in (b), $\hat{r}_c \equiv \hat{z}$.

Next consider the component of the torque in (b) that acts in the z direction (which in this configuration is also referred to as the centroid direction $\hat{r}_c$). This represents the component of a torque vector that tends to spin the plate around the centroid. We refer to this as the radial component of the torque due to $\vec{F}_n$. This radial component of the torque has a moment arm length of $r_0\sin(\varphi)$ where φ is the angle between the centroid and the boundary where the force is located. As in the planar case, this component of the torque has an intrinsic dependence on the distance between the point force and the centroid (or z axis). Note that in the case of a very small plate, we can use the small angle approximation ($\sin(\varphi) \approx \varphi$) in which case, the z component of the torque depends on $r_0\varphi \approx y$, i.e the torque is simply proportional to the distance from the z axis, as in the planar case.

The brown arrow shown in (b) is the component of the force that gives rise to the torque component around the y axis. This also produces purely tangential motion at the centroid. Again, this is analogous to the effect of the net linear force in (a), given by the component of force acting orthogonal to the centroid direction. The moment arm length is given by $r_0\cos(\varphi)$, or by r_0 in the small angle approximation.

As shown in Fig. 4, the radial and tangential components of the torque can be written in terms of (1) the angle between the plate boundary normal and the centroid direction (θ) and (2) the angle between the location where the point force acts and the centroid (φ):

$$\begin{aligned}\vec{\tau}_{\text{rad}} &= -|\vec{F}_n|r_0\ \sin(\theta)\ \sin(\varphi)\,\hat{z}\\ \vec{\tau}_{\text{tan}} &= -|\vec{F}_n|r_0\ \cos(\theta)\,\hat{x}\\ &\quad+|\vec{F}_n|r_0\ \sin(\theta)\ \cos(\varphi)\,\hat{y}\end{aligned} \tag{6}$$

The tangential component of the torque can also be described by an equivalent force acting at the centroid (e.g., Becker & O'Connell, 2001):

$$\vec{F}_{eq} = (\vec{\tau}_{\text{tan}}\times\hat{r}_c)/r_0 \tag{7}$$

Because the surface of a sphere is locally flat, the description of the spherical case must be identical to the planar case for a small plate. This can be verified by applying the small angle approximations (for φ) to the tangential and radial components of the torque, and representing the former as an equivalent force. Based on these considerations we refer to the tangential and radial components of the torque vector as fictitious and true torque components.

For the radial component of plate driving/resisting torques, the magnitude of the torque depends on two aspects of the geometry: the azimuth of the plate boundary relative to the centroid (i.e. the component of the force that is normal to the centroid direction ($\sin(\theta)$), and also the angle (distance) between the plate centroid and the boundary ($\sin(\varphi)$). Hence, plate boundary normal forces that are perpendicular to the centroid direction, and are a long way from the centroid (i.e. $\sin(\varphi), \sin(\theta) \to 1$) have the greatest potential to impact the radial component of torque. In the following section we extend these generic ideas to the case of the Zealandia and the IBM margin in the Eocene.

Parameter name	**Type**	**Symbol**	**Units**
Earth mean radius	scalar	r_0	km
Earth radius vector	vector	$\vec{r}_0$	km
Earth radius unit vector	vector	$\hat{r}_0$	-
Plate boundary normal vector	vector	$\hat{n}$	-
Plate boundary normal force density†	scalar	F_n	TN/m
Plate boundary normal point force	vector	$\vec{F}_n$	TN
Plate centroid unit vector	vector	$\hat{r}_c$	-
Angle btw $\hat{n}$ & centroid direction	scalar	θ	rad.
Angle btw boundary point & centroid	scalar	φ	rad.
Rotation vector	vector	$\vec{\omega}$	$^\circ$/Ma
Radial rotation unit vector ‡	vector	$\hat{\omega}_{\mathrm{rad}}$	$^\circ$
Angle btw centroid and Euler pole	scalar	γ	$^\circ$

Table 1. Quantities and symbols used in the paper. † We discuss both dimensionless and dimensional values for plate boundary normal forces. Where dimensional values are used, the units will generally be expressed as TN, or $\mathrm{TN\,m^{-1}}$. ‡ See Section 4 for a description of units and how $\hat{\omega}_{\mathrm{rad}}$ is visualised.

3.2 Application to Pacific Plate at 47 Ma

We now highlight the key ideas from the previous section, in the context of the Pacific Plate boundary configuration at the Eocene transition; the purpose here remains primarily conceptual (the main results being presented in Section 4). Fig. 5 shows the tectonic configuration at 47 Ma, rotated so that the Pacific Plate geometric centroid lies along the z axis of a Cartesian coordinate system, and so that the arc that connects the centroid to a point on the IBM trench lies in a plane defined by the y-z axes (i.e. the centroid direction, as shown with a thin blue line). This rotation places the Pacific Plate, and the IBM margin, into a similar configuration as has been shown in the generic case in Fig. 4b. In the right hand panel of Fig. 5, the force due to slab pull at the IBM is represented as a point force acting in a margin normal direction (shown schematically with a green arrow). The net torque vector associated with a margin-normal point force at the center of the IBM margin is shown with the green arrow at the centroid location. The decomposition of the torque vector around the Cartesian axes is shown with the coloured arrows, as discussed in the Figure caption. Importantly, one can see that the radial component (black) is of similar magnitude to the components that contribute to the tangential torque (blue and brown).

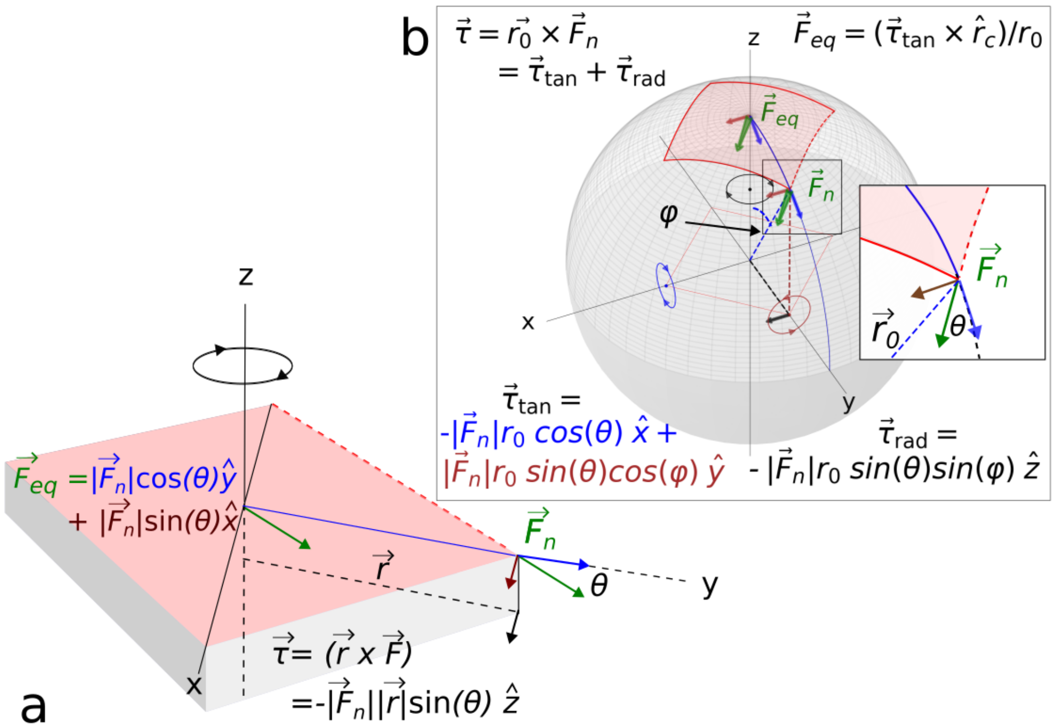

Figure 4. Effect of an arbitrary point force $\vec{F}_n$ acting on a square plate confined to (a) a planar surface and (b) the surface of a sphere: (a) shows the familiar case of a point force acting on a rigid body, contributing to a net force and a torque around the center of the object. $\vec{F}_n$ acts at the corner of the square plate, in a direction parallel to the edge of the square outlined with the dashed red line, and normal to the adjacent edge. The blue and brown arrows show the components of the force that are parallel and perpendicular to the centroid direction. The components of the net force ($\vec{F}_{\mathrm{eq}}$), and the torque (τ) are written as a function of θ, the angle between the point force on the boundary and the centroid direction. For the configuration represented here, $\theta = 45°$, but the relationships we derive are general; (b) shows the equivalent situation for a square plate on the sphere. In the traditional descriptions, $\vec{F}_n$ is associated with a torque (τ) around Earth's centre, as in Eq. 5. This torque vector has components in the x, y, and z directions. The z direction is aligned with the vector that points radially outward at the plate centroid ($\hat{r}_c$). We refer to the component of the torque in the z (or $\hat{r}_c$) direction, as the radial component of the torque; this is the true torque component, which is analogous to the usual definition of the torque as in case (a). For small plates (where the small angle approximation for φ is valid), the descriptions of the mechanics in (a) and (b) are identical, as discussed in the main text.

In addition, Fig. 5 shows the orientation of a putative boundary-normal collision resistance force at Zealandia (shown schematically with the red arrow). To simplify the figure, we have not shown the full decomposition of this point force, but only the projection of the point force onto the hemispheric plane (also with a red arrow). This evidences the capacity for a plate boundary normal force at the Zealandia margin to produce a radial component of torque, primarily because angle between the centroid direction and the boundary normal (i.e. θ) is large. The key insight from Fig. 5 is that plate boundary normal forces acting along both the IBM and Zealandia margins, are expected to be relatively effectively partitioned into the radial component of the torque on the Pacific Plate. In addition, the radial torque components are complimentary – both having a CCW sign (when looking down on the Pacific centroid). In fact, these two boundaries act in the sense of a force couple, as the tangential torque component of collision resistance along the Zealandia margin would tend to oppose the tangential component of torque due to the IBM margin.

3.3 Assumptions in the estimation of torque components

Having discussed the general aspects of torques due to plate boundary forces, we conclude this section with some methodological details in applying this framework to plate reconstruction models. In this study we restrict our attention to putative plate boundary normal forces that arise from Pacific Plate subduction margins, as well as the potential collision resistance from the intra-continental Zealandia margin.

Eq. 6 provides a means of calculating the radial and tangential components of the torque, in a rotated reference frame, which is instructive for understanding torque partitioning due to a point force. However, for the general analysis we simply calculate a net torque (τ_{net}) as the sum of torque increments in a fixed Cartesian coordinate system (as in Eq. 4). The radial and tangential components are calculated using projections onto the centroid vector (identical to Eq. 1 for the rotation vector). We compute the torque components both in terms of the net Pacific Plate subduction margin torque, and at the level of regional margin segments (e.g. IBM, Tonga, Aleutian etc.). The location and extent of these regional segments, at several times, is shown in Supplementary Fig. S4.

The analysis does not account for the age of the subducting plate in terms of the predicted slab pull force, and is purely based on geometric information. In keeping with this assumption, the calculations are based on the geometric centroid of the Pacific Plate, rather than attempting to estimate the center of mass. The centroid locations are shown in Fig. 1, and remain relatively stationary across the Cenozoic. The torque values in Fig. 6 are non-dimensionalised by assuming a reference torque $\tau_{\mathrm{ref}} = F_n {R_e}^2$. The torque calculations (e.g Eq. 3) are scaled by τ_{ref}, such that the magnitude of F_n is not actually specified in our calculations. Hence, the estimated torque values discussed in the following section (e.g. Fig. 6) represent geometric information only.

In the reconstruction of Müller et al. (2016), the IBM subduction margin appears at 55 Ma. However, geological evidence from the age and composition of initial magmatism, both in forearc and backarc regions, places the initiation age somewhat later at ca. 52 Ma (Ishizuka et al., 2006, 2011; Arculus et al., 2015). This issue has been highlighted in the recent study of Hu et al. (2022b), which focuses on the drivers of the rapid change in the azimuth of the Pacific plate (effectively the tangential part of the rotation). That study proposes that: 1) the IBM initiation probably occurs somewhat later than the Müller et al. (2016) model represents; and 2) the development of a slab pull force is delayed for a further several million years, representing the time taken for the accumulating upper mantle slab density to begin to dominate over forces resisting subduction (such as bending, interplate friction etc.)

In light of these insights, our subduction margin analysis makes the following assumptions: Firstly, we use an updated plate geometry model (Hu et al., 2022b), which is based on the Müller et al. (2016) model, but includes additional north-dipping Pacific Plate subduction prior to 47 Ma (the Kronostsky margin). Secondly, we delay the IBM initiation time to 52 Ma. Thirdly, we introduce a lag phase of 5 Ma, such that forces associated with new subduction margins do not immediately act on the trailing (e.g. Pacific) plate. This applies to all initiating subduction zones across the Cenozoic. Our analysis only includes 'outward' Pacific Plate subduction margin segments; where other plates subduct inward under the Pacific Plate (such as the Puysegur margin, south of New Zealand) these are not included in the torque calculation.

To estimate the torque contributions due to collision resistance at the Zealandia margin, we have made a few further simplifying assumptions. We assume collision resistance forces (F_c), with a specified, constant magnitude operated throughout the pivot period (ca. 47-32 Ma), before and after which they were absent. During the pivot period, we model the collisional Zealandia margin as a 1000 km segment which is perfectly parallel to the centroid direction. This means that the plate boundary normal force is orthogonal to the centroid direction, or $\theta = 90°$ (see Fig. 5). The length of intra-continental boundary, parallel to the centroid direction, is on the order of 1000 km, as shown in Supplementary Figure S5. Under these assumptions (e.g. $\theta = 90°$), the 47 Ma intra-continental Zealandia margin, has a radial/tangential ratio of ~ 1.5 (from Eq. 6 this ratio is equal to $\cos(\varphi)/\sin(\varphi)$, and corresponds to φ of 56 °). The implication is that the Zealandia margin would have predominantly partitioned plate boundary normal forces into a (CCW) radial torque component.

In the following sections we will refer to the magnitude of plate boundary force densities (forces per unit length, e.g., TN/m) that arise from subduction margins as F_{sp}, and those that arise from the Zealandia collisional margin as F_c. We denote the ratio of these force densities as $F_R = F_c/F_{sp}$.

4 Results

4.1 Evolution of Pacific Plate torque components

Fig. 6 shows the radial and tangential torque components, associated with Pacific Plate subduction margins, and Zealandia margin collision, based on assumptions discussed in the previous section. The solid black lines in Fig. 6 show the estimated net subduction-related torque components, while the colored circles show the contributions of individual subduction margins (e.g., IBM, Tonga, etc.). Several new subduction margins initiate prior to the Eocene transition, (IBM, Japan and Kurile) as shown in Fig. 6A. This is reflected in a significant increase in the magnitude of the tangential torque component between about 55-47 Ma, shown with the solid black line in Fig. 6B. For the remainder of the Cenozoic, the predicted magnitude of the tangential torque component remains quite stable, with an average dimensionless value of around 1.4.

Fig. 6B reveals that the tangential component of the subduction margin torques are broadly constructive, as shown by the fact that the magnitude of net tangential torque is usually significantly larger than any of the individual regional components. However, also note that the total tangential torque (solid black line Fig. 6B) is the *vector sum* of the boundary contributions, it is not the sum of the magnitudes of the regional segments (which is shown with the thin black line). The difference between the solid and dashed lines represents the level destructive interference, typically amounting to about $\frac{1}{3}$ of the total, and varying somewhat over time. An example of the vector nature of the torque contributions is given by the cessation of the Melanesian subduction which occurs at ca. 12 Ma. The cessation of subduction along this margin is calculated to have had very little impact on the magnitude of the total tangential torque (thick black line), because the

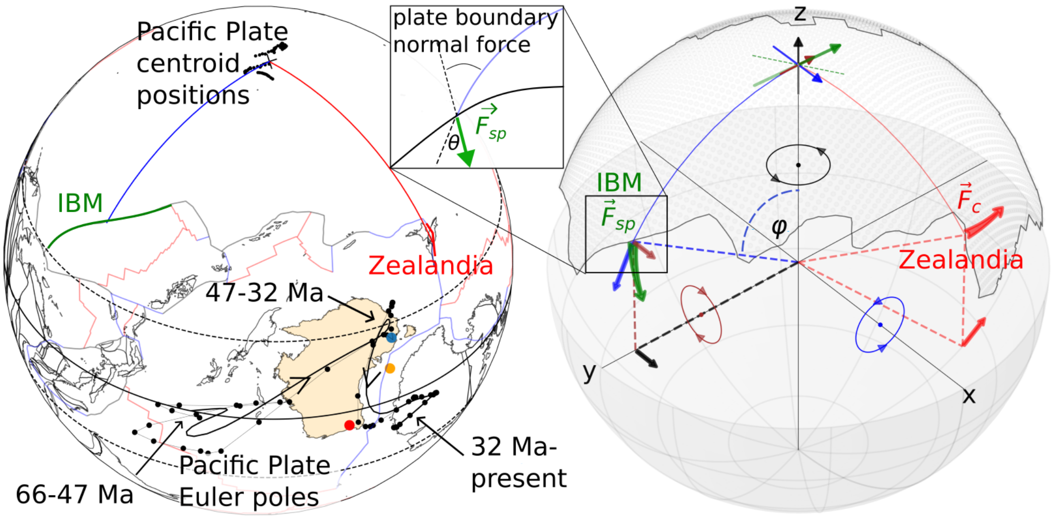

Figure 5. Schematic showing how different torque components are generated from plate boundary forces. Both panels show the tectonic configuration at 47 Ma. Globe is rotated so that the Pacific centroid lies at the pole (along the z-axis) while the arc from the centroid to the IBM margin lies in y-z plane. Left panel shows the Pacific Plate Euler poles relative to the reference frame (black points). The right panel shows a schematic representation of plate boundary normal forces, for subduction at the IBM margin (green) and collision resistance at Zealandia margin (red). The blue, brown and black arrows show how the point force normal to the IBM margin would contribute to three orthogonal torques. The component of the point force acting in the centroid direction (in the same plane as the y-axis) produces a torque around the x-axis (blue symbols). This is a pseudo-torque because it has no dependence in the angle φ. The component of the force orthogonal to the centroid direction produces a radial torque (a 'true' torque) around the z-axis (or centroid axis). Both the IBM and Zealandia margins are expected to produce significant CCW radial torques on the Pacific Plate.

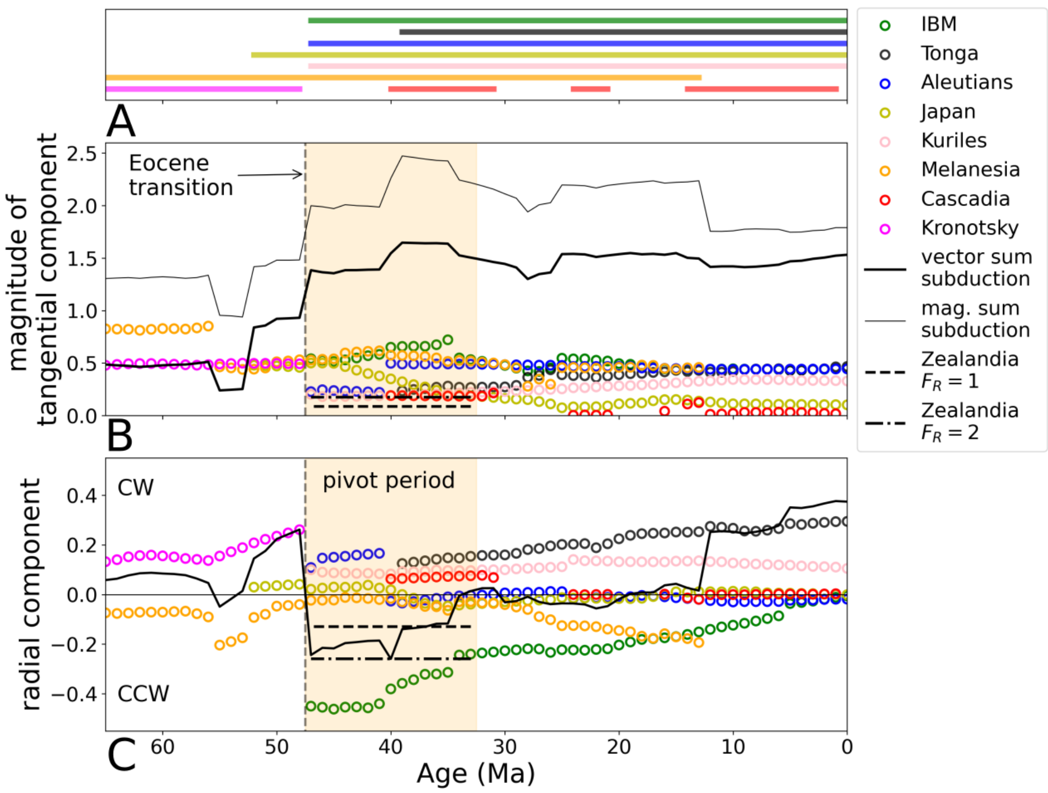

Figure 6. Evolution of torque components due to Pacific Plate subduction margin forces, based on the plate reconstruction model of Müller et al. (2016), incorporating an updated Pacific subduction margin model of Hu et al. (2022b). Torque values are dimensionless, as discussed in the main text. Colored circles show the contribution of regional subduction zones, such as the IBM margin, as labelled in the legend. The top panel (A) shows the duration of the regional subduction segments. (B) shows the magnitude of the tangential torque components. The vector sum of the regional torque contributions is shown with a solid black line, while the dashed black line is the sum of the magnitudes of the regional torque contributions. (C) shows radial torque components; in this case the vector sum (solid black line) is equal to the sum of the magnitudes of regional contributions, because the radial torque components are always parallel. Also shown here are the estimated contributions of the Zealandia margin, during the pivot period, under 2 assumptions about the relative ratio of collision to subduction-related force densities, as discussed in Section 3.3. F_R=1 is shown with the thick dashed line, and where Zealandia collisional forces were assumed to be equal the magnitude of subduction-related forces. F_R=2 is shown with the thick dot-dashed line, where collisional forces are twice the magnitude of subduction margin forces.

south-dipping orientation of the Melanesian margin produced a regional torque contribution that was near-perpendicular to the total torque (see Supplementary Fig. S4). However the cessation of subduction is clearly evident in the sum of magnitudes of the regional torque contribution (thin black line).

Fig. 6C shows the radial component of the estimated torques acting on the Pacific Plate. There are two key insights we draw from this plot. First is that the IBM margin – during the pivot period – has the largest predicted radial torque contribution of any regional segment of the subduction margin at any time throughout the Cenozoic. During this peak, the radial component of the IBM margin is more than twice the magnitude of the next largest regional component (Aleutian margin), and exhibits a maximum radial/tangential torque ratio of ~ 0.9 (i.e. almost equal partitioning). Secondly, the estimated radial torque components tend to exhibit significant destructive interference (in contrast to the tangential torques). For instance, the net radial torque is close to zero in the interval ca. 32-12 Ma, due to the opposing radial torque contributions of individual segments, such as IBM (CCW) and Tonga (CW) margins. This attribute of the radial torque contributions has implications for the relative impact of additional forces, such as from the Zealandia margin. Overall, there is a broad trend from a CCW radial component beginning at the Eocene transition, when the IBM margin dominated the radial torque, to a CW rotation torque component during the past ca. 12 Myr, where Tonga dominates. Note that progressive, differential, trench rollback in these 2 segments has followed an opposite trajectory, as far as the magnitude of the radial torque is concerned. Along the IBM margin, rollback has decreased the θ angle, partitioning ever-less force into the radial component of the torque, while the opposite is true for the Tonga margin.

The dashed and dot-dashed lines in Fig. 6 show the estimated torque contributions for Zealandia, based on assumptions about the boundary geometry discussed in the previous section. Two cases are shown, 1: where the Zealandia margin force density is assumed to be the same as that of the subduction margins (i.e. $F_R = 1$, dashed line), and 2: where the Zealandia margin is 2 times larger than the latter (i.e. $F_R = 2$, dot-dashed line). Under either assumption, the contribution of Zealandia to tangential torques is significantly smaller than the net effect of subduction margins. This point will also be seen in Fig. 7, where we consider the (vector) addition of the torque components due to Zealandia and the net torque due to subduction. The simple conclusion is that under the assumptions represented in Figs. 6&7, Zealandia does not amount to a first-order contribution in terms of the tangential torque.

In terms of radial torques, the impact of Zealandia may be much more significant. Indeed, we see that the two respective assumptions about F_R (dashed and dot-dashed lines, in Fig. 6) lead to radial torque contributions that bound the net radial torque contribution of the subduction margins (shown with a solid black line). Note, however, that even under the stronger assumption about collisional forces ($F_R = 2$), the IBM margin is still the largest single contributor to radial torques. This is because the IBM margin is about 4.5 times longer that the assumed length of the Zealandia margin (1000 km). However, the radial torque contribution of the IBM margin is buffered the tendency of most other subduction margins to pull in a CW sense. The destructive interference in radial subduction torques amplifies the contribution of the Zealandia margin.

4.2 Comparison of torques and Pacific Plate motion changes

Fig. 7 shows a comparison between rotation components (in green) and dimensionless torques (in black). The vertical scales have been arbitrarily chosen so that the rotations (left axis) and torques (right axis) have similar total variation. In examining potential correlations, it is important to consider the geodynamic framework discussed in the final paragraph of the introduction, regarding the drivers of rapid plate motion changes.

A specific implication of this framework is that torques due to subduction and collision represent only a partial description of the overall plate equilibrium. Therefore, we would not expect perfect alignment between plate rotation vectors and torque vectors due to subduction/collision. However, we would expect to see an overall consistency between rapid changes in subduction/collision torques and similarly-rapid changes in rotation. For, instance, if torque changes imply a CW change in the plate azimuth at the centroid, we would expect a similar CW change in plate rotation, although both the absolute values and the relative magnitude of the change may differ, which would represent the presence of additional forces in the overall plate equilibrium. In Fig. 7A, we can see that prior to the Eocene transition, the azimuth of the Pacific Plate is poorly predicted by subduction related torques (e.g. Fig. 7A). This is despite inclusion (in our calculations) of an updated model for northern Pacific Plate subduction margins (Hu et al., 2022b). This lack of correlation, however, may simply represent the fact that additional forces, e.g. due to long-wavelength flow, provided a northerly-oriented force component. Indeed this is the explanation advanced by previous studies, which have noted a similar mismatch in this time period (Faccenna et al., 2012). The numerical model results, which we discuss later in this section, support this interpretation.

Figure. 7 suggests that there two Cenozoic events (47 Ma and 12 Ma), in which we see consistent changes between components of Pacific Plate rotation and subduction torques. We have already commented on the subduction-margin reconfiguration that occurred prior to the Eocene transition, including initiation of the IBM subduction zone. Changes in estimated subduction torque at 47 Ma, are consistent with the sign of the changes in rotation components. However, the radial component exhibits the clearest correlation, in that both the sign and relative magnitude of the change exhibit closer similarity: in each case, the Eocene transition represents the single largest radial change across the Cenozoic.

The change in torque components at about 12 Ma is associated with the cessation of southward dipping subduction at Melanesia. The geodynamic context is the collision of the Ontong Java Plateau, potential slab breakoff and subduction polarity reversal. A previous study, based on dynamic modelling, has proposed a link between the collision and the observed northwards change in Pacific Plate velocities in this period (although it was based on a plate reconstruction that puts the timing of the collision somewhat later (Austermann et al., 2011)). Our analysis provides the additional insight that this change involved both the tangential azimuth (Fig. 7A) and, to an even greater (relative) degree, the radial rotation component of rotation/torque (Fig. 7C). The only component of this ca. 12 Ma change that is not consistent, in terms plate rotation versus torque estimates, is the magnitude of the tangential change (Fig. 7B). However, in both cases changes in this component are small compared to the relative change in the other 2 components. Hence we view this inconsistency as being of minor importance.

Overall, however, there remain several aspects of Cenozoic Pacific Plate rotation which are not correlated with patterns in estimated torques. Importantly, this includes instances of rotation changes that are rapid in nature. For instance, consider the rapid decrease (and reversal) of the CCW radial rotation component at the end of the pivot period (ca. 32 Ma) shown in green line Fig. 7C. While subduction torques predict a decrease in the CCW component across the pivot period, the rapid nature of this change is not predicted.

Furthermore, subduction-related torques do not provide an explanation for many of the rapid changes in the magnitude of the tangential component of Pacific Plate velocity (Fig. 7B), such as those which occur at ca. 60, 40, & 28 Ma. The change in tangential rotation magnitude, at 40 Ma, is worth highlighting as it exhibits neither a corresponding change in the azimuth of the plate at the centroid (Fig. 7A), nor in the radial rotation component (Fig. 7C). This represents a case of a reduction in the tangential rotation rate, but negligible change in the rotation axis. These changes would seem

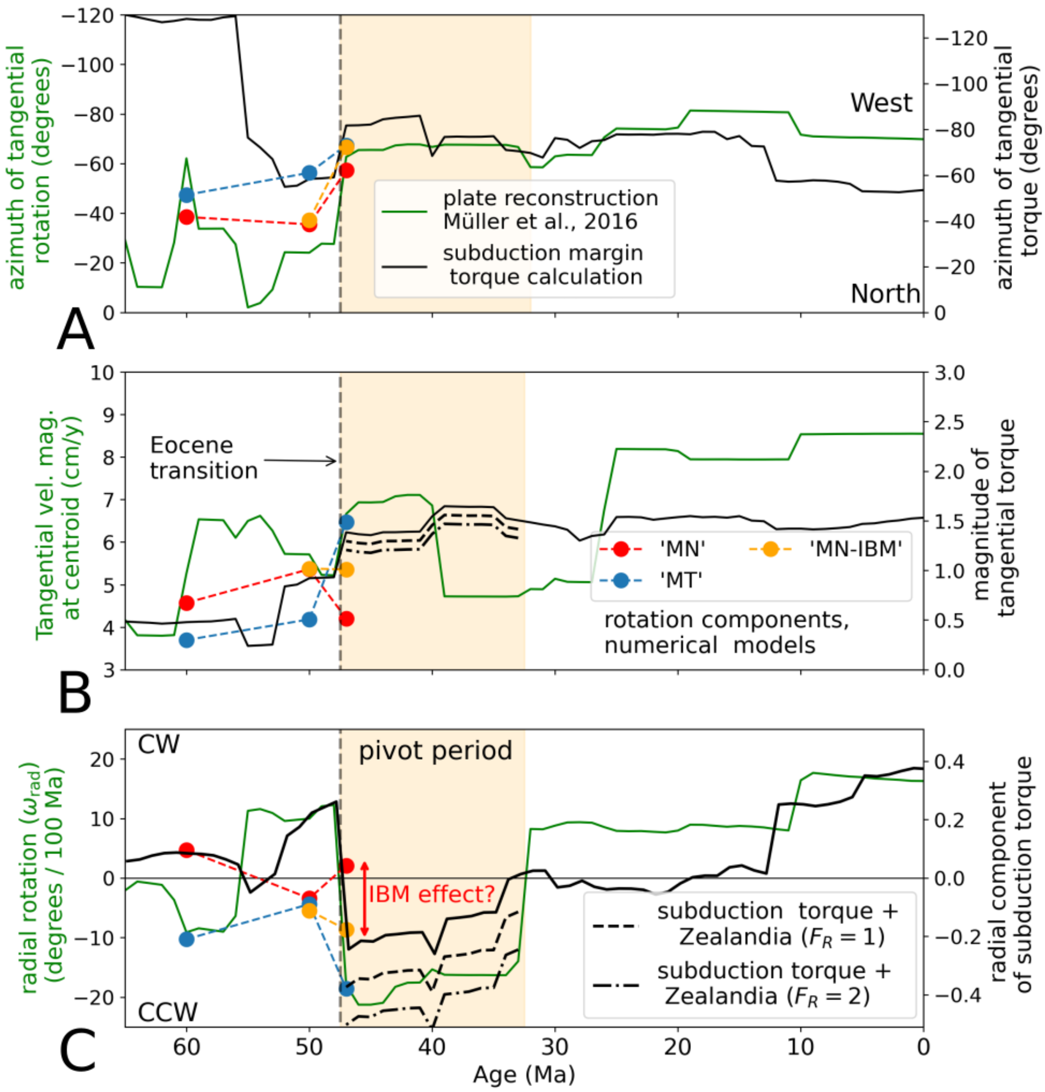

Figure 7. Comparison between estimated subduction related torques and components of the Pacific Plate rotation vector. Green line show plate rotation components as based on Müller et al. (2016)(see Fig. 3 caption for further details). Net subduction torque components are shown with solid black lines, as in Fig. 6. The dashed and dot-dashed line segments show estimated torque contributions of the Zealandia margin, added to the total subduction related torques. Zealandia opposes the tangential torque of the subduction margins, but compliments the CCW radial rotation. Two scenarios are shown, F_R=1, and F_R=2, as discussed in Section 4. The colored circles show rotation components from global-scale numerical models of Hu et al. (2022b). The difference between the 'MN' and 'MN-IBM' models provides an estimate of the effect of the IBM margin. This is shown with the vertical red arrow, labelled 'IBM effect?' in the bottom panel (C). The corresponding difference in azimuth (top panel) is less significant (as discussed in Hu et al. (2022b)).

to imply a slowdown of the system, while the relative magnitudes of driving/resisting forces remain constant (hence no shift in the rotation axis). Our analysis suggests there is nothing in the evolving geometry of the Pacific Plate subduction margin that could account for this change. Moreover, rapid changes in regional subduction margins tend to produce changes in plate direction and/or radial rotation (47 Ma and 12 Ma). While rapid changes in plate motion are often attributed to the rapid evolution of subduction margins, it seems difficult to account for the 40 Ma slowdown in that context.

Subduction margin-related torque changes can provide an explanation for some – but not all – of the rapid changes in Cenozoic Pacific Plate motion (as represented in plate reconstruction models of Müller et al. (2016)). Fig. 7 also shows how putative collisional forces along the Eocene Zealandia margin might have impacted the torque balance. In evaluating the potential contribution, there are two basic questions to assess: 1) is it plausible that collision resistance forces along the Zealandia margin could have a first order impact on Pacific Plate torques? And 2: does the nature of these torques contributions have explanatory power in terms of observed rotations? Note that in Fig. 7, we show the effect of Zealandia margin forces under the assumptions that such forces operated with a constant magnitude within the pivot period, but were otherwise absent. This is, of course, a major simplification. However, our approach is intended simply to assess the relative capacity of the Zealandia margin to affect Pacific Plate torques during the pivot period.

As previously discussed, the assumption of $F_R = 1$, already implies that Zealandia would have had a first-order effect on the radial component of Pacific Plate torques, relative to the net subduction component. F_R of ~ 2, makes the total (subduction plus collision) radial torque during the pivot period higher than at any other stage during the Cenozoic; this assumption can therefore account for the similar peak in radial rotation rate. A further assumption – that Zealandia collision resistance rapidly reduced at around 32 Ma – helps to explain the rapid reduction in the (CCW) radial radial rotation at the end of the pivot period, which subduction margin forces alone cannot account for. During this period, the Zealandia margin evolves from the stage of pivoting, where the Pacific-Australian Euler pole lay on the plate boundary (Sutherland, 1995), to a mature transform boundary, as Zealandia moved NW away from the Euler pole (as viewed relative to the absolute reference frame, e.g. Fig. 2). During such an evolution, it is conceivable that a rapid change in boundary-normal forces – an kind of unlocking process – may have occurred. However, such a transition (at about 32 Ma) is speculative, and should be considered as such.

4.3 Insights from global geodynamic models

Even when modified to try to better represent dynamic process (such as a subduction initiation lag), the use of parameterised plate boundary forces has obvious limitations (Becker & O'Connell, 2001). The results from global-scale numerical models provide an alternative opportunity to establish potential links between evolving plate boundaries, and plate motion changes. A recent example of this approach is demonstrated in Hu et al. (2022b), which compares two alternative models for the subduction boundary evolution of the Pacific Plate.

The reference model ('MT') presented in Hu et al. (2022b) is based on the plate reconstruction of Müller et al. (2016), while an alternative model ('MN') includes a several-thousand kilometer north-dipping intra-oceanic 'Kronotsky' subduction, which is active until 50 Ma. This alternative model is run both with ('MN-IBM') and without ('MN') subduction at the IBM margin. It should be noted that in all cases, the lithospheric structure includes the new Pacific-Australian plate boundary through Zealandia (from 47 Ma). The models can, in principle, accommodate deformation and collision resistance across the Zealandia margin. However, the models do not include features such as a strong, buoyant, underthrust Hikurangi Plateau, which could limit how accurately they will capture collision resistance across such a boundary (e.g., Reyners, 2013). Surface velocity fields for the models of Hu et al. (2022b) were provided in the original study, from these we estimated Euler poles based on least squares fitting. Based on these results we make the following observations:

1. In both models (MT and MN) the Pacific Plate exhibits a NW velocity azimuth at 60 Ma (-40 °, e.g., Fig. 7A). This is nearly orthogonal to the calculated azimuth based in the torque due to subduction-related normal forces, based on the same plate reconstruction (-120 °). We interpret this as suggesting that other driving forces (along with direct slab pull) play an important role (as was suggested by Faccenna et al. (2012) for times prior to about 60 Ma).
2. The inclusion of subduction along the IBM margin produces a significant CCW effect on the radial component of the rotation. This observation is primarily deduced from the model setups that are identical except for the inclusion the IBM margin (MN-IBM & MN: shown as yellow and red circles in Figs. 1&7). This difference in these models is represented by the red labelled arrow in Fig. 7C.
3. The change in the Pacific Plate Euler pole location at 47 Ma, due to the inclusion of the IBM subduction zone (initiating at 5 Ma), is along an arc that points almost directly towards Zealandia. This can be seen by comparing the Euler poles shown with the red and yellow circles in Fig. 1.
4. When the IBM margin is not included, the Pacific plate at 47 Ma has negligible radial rotational component (e.g. 'MN' model, red symbol in Fig. 7C). In this model, there is no residual CCW 'signal' which might be identified with the effect of the Zealandia margin, independent from the effect of subduction at the IBM margin.

In summary, the models of Hu et al. (2022b) suggest that: (1) Pacific Plate motion is sensitive to the structure of the subduction margins, although other driving forces may be equally important; (2) the inclusion of subduction initiation at the IBM margin (at 51 Ma) has a relatively large impact on the radial rotation component (at 47 Ma), which is consistent with our geometric analysis; (3) The absolute motion changes induced by the IBM margin would in turn seem to facilitate Pacific-Australian (relative) pivoting, as they move the Pacific Plate Euler pole towards Zealandia.

5 Discussion and conclusions

This study is fundamentally concerned with the relative and absolute motions of the Pacific and Australian plates, spanning the period of rapid tectonic reorganisation at ca. 50 Ma (The Eocene transition). This transition involves the frequently-discussed westwards change in Pacific Plate absolute motion. Another aspect, which has been comparatively overlooked, is that Pacific Plate rotation also developed a relatively high radial component (CCW sense). Moreover, this period of high radial rotation (ca. 47 - 32 Ma, as inferred in Müller et al. (2016)), overlaps a similar interval wherein the relative Pacific-Australian rotation axis was situated within continental Zealandia (Sutherland, 1995). Altogether, this sequence of events suggests that forces originating at the Zealandia margin could have played an important role in the evolving Pacific Plate torque balance, along with those associated with the evolving subduction margin, which have been a major focus of previous investigations (Whittaker et al., 2007; Faccenna et al., 2012; Hu et al., 2022b).

Our torque analysis, along with results from numerical models, highlights the role played by the IBM margin in the Eocene transition. In particular, the configuration of the IBM margin leads to an anomalous impact on the radial component of torques (and rotations in the case of the numerical models of Hu et al. (2022b)). This radial contribution of the IBM has not been recognised in previous studies, which have – in a sense

– underestimated its overall importance (Hu et al., 2022b). Because of its geometric configuration, Zealandia is even more efficient in terms of partitioning plate boundary normal forces into CCW radial torques. Hence, Zealandia provides a 'push in the right direction'. While both the IBM and Zealandia margins have strong potential for explaining the CCW radial components of Pacific Plate rotation, additional assumptions are required to make definitive statements about the relative contributions. In this study, such assumptions are encapsulated in the value of F_R, being the relative force density of collision resistance versus typical subduction margins. We show that $F_R \sim 1$ is sufficient for Zealandia to represent a first order contribution to the radial component of the Pacific Plate torque balance. In Section 4, we posed the question is this ($F_R \sim 1$) a plausible value?

Investigations in numerous settings have concluded that collisional margins may produce force densities larger than typical subduction related forces (England & Houseman, 1986; Cloetingh & Wortel, 1986; England & Molnar, 2022; Reynolds et al., 2002). Many such estimates relate to regions of significant crustal thickening, and associated gravitational potential energy forces (e.g. Himalaya/Tibet, Andes); hence the applicability with the Eocene Zealandia margin might be limited. However, significant Eocene shortening and uplift are recorded in Zealandia, such as $\sim$ 12-15 km of motion of the Taranaki Fault beginning around 40–43 Ma (Stagpoole & Nicol, 2008), as well as the distributed deformation of Zealandia that has recently been documented (Sutherland et al., 2020). Hence regional geological evidence is consistent with significant deviatoric compression across the northern part of Zealandia. We also note that the modern day Zealandia margin (Alpine Fault - Southern Alp System) is thought to transmit margin normal force densities of about 3 TN/m (Reynolds et al., 2002; Sandiford et al., 2004), i.e. of similar magnitude to inferred net slab pull in several previous studies (Forsyth & Uyeda, 1975; Schellart, 2004; Bird et al., 2008; Copley et al., 2010; England & Molnar, 2022). Overall, the proposition of equivalent force densities between subduction margins and collisional margins is certainly plausible in terms of additional tectonic settings.

As we have shown, both radial and tangential changes in absolute Pacific Plate motion appear to have facilitated relative Pacific-Australian Euler poles locating close to Zealandia during the pivot period. Boundary normal forces along Zealandia have relatively little impact on the Pacific Plate tangential torques, compared to the integrated effect of subduction margins. Our analysis suggests that the onset of Pacific-Australian pivoting (at ca. 47 Ma) was tied to broader changes in the plate driving/resisting forces, including far-field subduction zone reconfiguration, rather than being dominated by forces arising proximal to the pivot point, i.e. collision resistance within the intra-continental Zealandia margin. Nevertheless, it is plausible that forces along the Zealandia margin played a contributing role in the anomalously high Pacific Plate radial rotation during the pivot period. Moreover, rapidly evolving forces in the Zealandia margin, could help to explain features that are not readily explicable in terms of subduction torques alone, such as the rapid decline in radial rotation at about 32 Ma. This suggestion remains speculative however, and will require further analysis. Important insights may be gained from analysing global convection models, such as those presented by Hu et al. (2022b), in terms of a radial/tangential rotation decomposition.

6 Open Research

Data: Velocity grids from numerical models of (Hu et al., 2022b) are available at Caltech Data (`https://doi.org/10.22002/D1.2150`) (Hu et al., 2022a)
Software: Geographical figures were made with GPlately (`https://doi.org/10.1002/gdj3.185`) (Mather et al., 2023).

Acknowledgments

PyGplates and gplately (Mather et al., 2023) software (www.gplates.org) are funded by the AuScope infrastructure-development programme. The work was supported by Australian Research Council grants DP150102887 and DP180102280. The research was facilitated by the flexible and supportive Post Doctoral position provided by Monash University and the aforementioned grants. We would like to thank Dr. Bernhard Steinberger as well as an anonymous reviewer for their constructive comments and attention to detail.

References

Arculus, R. J., Ishizuka, O., Bogus, K. A., Gurnis, M., Hickey-Vargas, R., Aljahdali, M. H., ... others (2015). A record of spontaneous subduction initiation in the izu–bonin–mariana arc. *Nature Geoscience*, *8*(9), 728–733.

Austermann, J., Ben-Avraham, Z., Bird, P., Heidbach, O., Schubert, G., & Stock, J. M. (2011). Quantifying the forces needed for the rapid change of pacific plate motion at 6 ma. *Earth and Planetary Science Letters*, *307*(3-4), 289–297.

Becker, T. W., & O'Connell, R. J. (2001). Predicting plate velocities with mantle circulation models. *Geochemistry, Geophysics, Geosystems*, *2*(12).

Bird, P., Liu, Z., & Rucker, W. K. (2008). Stresses that drive the plates from below: Definitions, computational path, model optimization, and error analysis. *Journal of Geophysical Research: Solid Earth*, *113*(B11).

Cloetingh, S., & Wortel, R. (1986). Stress in the indo-australian plate. *Tectonophysics*, *132*(1-3), 49–67.

Colli, L., Stotz, I., Bunge, H.-P., Smethurst, M., Clark, S., Iaffaldano, G., ... Bianchi, M. C. (2014). Rapid south atlantic spreading changes and coeval vertical motion in surrounding continents: Evidence for temporal changes of pressure-driven upper mantle flow. *Tectonics*, *33*(7), 1304–1321.

Copley, A., Avouac, J.-P., & Royer, J.-Y. (2010). India-asia collision and the cenozoic slowdown of the indian plate: Implications for the forces driving plate motions. *Journal of Geophysical Research: Solid Earth*, *115*(B3).

Eberhart-Phillips, D., Reyners, M., Upton, P., & Gubbins, D. (2018). Insights into the structure and tectonic history of the southern south island, new zealand, from the 3-d distribution of p-and s-wave attenuation. *Geophysical Journal International*, *214*(2), 1481–1505.

England, P., & Houseman, G. (1986). Finite strain calculations of continental deformation: 2. comparison with the india-asia collision zone. *Journal of Geophysical Research: Solid Earth*, *91*(B3), 3664–3676.

England, P., & Molnar, P. (2022). Changes in plate motions caused by increases in gravitational potential energy of mountain belts. *Geochemistry, Geophysics, Geosystems*, *23*(10), e2022GC010389.

Faccenna, C., Becker, T. W., Lallemand, S., & Steinberger, B. (2012). On the role of slab pull in the cenozoic motion of the pacific plate. *Geophysical Research Letters*, *39*(3).

Forsyth, D., & Uyeda, S. (1975). On the relative importance of the driving forces of plate motion. *Geophysical Journal International*, *43*(1), 163–200.

Gaina, C., Müller, D. R., Royer, J.-Y., Stock, J., Hardebeck, J., & Symonds, P. (1998). The tectonic history of the tasman sea: a puzzle with 13 pieces. *Journal of Geophysical Research: Solid Earth*, *103*(B6), 12413–12433.

Gurnis, M. (2023). An evolutionary perspective on subduction initiation. In *Dynamics of plate tectonics and mantle convection* (pp. 357–383). Elsevier.

Hu, J., Gurnis, M., Rudi, J., Stadler, G., & Müller, R. D. (2022a). Data set for manuscript "dynamics of the abrupt change in pacific plate motion around 50 ma" [dataset].
doi: 10.22002/D1.2150

Hu, J., Gurnis, M., Rudi, J., Stadler, G., & Müller, R. D. (2022b). Dynamics of the abrupt change in pacific plate motion around 50 million years ago. *Nature Geoscience*, *15*(1), 74–78.

Ishizuka, O., Kimura, J.-I., Li, Y. B., Stern, R. J., Reagan, M. K., Taylor, R. N., ... others (2006). Early stages in the evolution of izu–bonin arc volcanism: New age, chemical, and isotopic constraints. *Earth and Planetary Science Letters*, *250*(1-2), 385–401.

Ishizuka, O., Tani, K., Reagan, M. K., Kanayama, K., Umino, S., Harigane, Y., ... Dunkley, D. J. (2011). The timescales of subduction initiation and subsequent evolution of an oceanic island arc. *Earth and Planetary Science Letters*, *306*(3-4), 229–240.

Keller, W. R. (2005). *Cenozoic plate tectonic reconstructions and plate boundary processes in the southwest pacific.* California Institute of Technology.

Lamb, S., Mortimer, N., Smith, E., & Turner, G. (2016). Focusing of relative plate motion at a continental transform fault: Cenozoic dextral displacement¿ 700 km on new zealand's alpine fault, reversing¿ 225 km of late cretaceous sinistral motion. *Geochemistry, Geophysics, Geosystems*, *17*(3), 1197–1213.

Mahoney, J., Storey, M., Duncan, R., Spencer, K., & Pringle, M. (1993). Geochemistry and age of the ontong java plateau. *The mesozoic Pacific: Geology, tectonics, and volcanism*, *77*, 233–261.

Mather, B. R., Müller, R. D., Zahirovic, S., Cannon, J., Chin, M., Ilano, L., … others (2023). Deep time spatio-temporal data analysis using pygplates with plate tectonic tools and gplately. *Geoscience Data Journal*.

Morgan, W. J. (1972). Plate motions and deep mantle convection. *Geological Society of America Memoirs*, *132*, 7–22.

Mortimer, N. (2018). Evidence for a pre-eocene proto-alpine fault through zealandia. *New Zealand Journal of Geology and Geophysics*, *61*(3), 251–259.

Müller, R. D., Seton, M., Zahirovic, S., Williams, S. E., Matthews, K. J., Wright, N. M., … others (2016). Ocean basin evolution and global-scale plate reorganization events since pangea breakup. *Annual Review of Earth and Planetary Sciences*, *44*(1), 107–138.

O'Connor, J. M., Hoernle, K., Müller, R. D., Morgan, J. P., Butterworth, N. P., Hauff, F., … Stoffers, P. (2015). Deformation-related volcanism in the pacific ocean linked to the hawaiian–emperor bend. *Nature Geoscience*, *8*(5), 393–397.

Reyners, M. (2013). The central role of the hikurangi plateau in the cenozoic tectonics of new zealand and the southwest pacific. *Earth and Planetary Science Letters*, *361*, 460–468.

Reynolds, S. D., Coblentz, D. D., & Hillis, R. R. (2002). Tectonic forces controlling the regional intraplate stress field in continental australia: Results from new finite element modeling. *Journal of Geophysical Research: Solid Earth*, *107*(B7), ETG–1.

Sandiford, M., Wallace, M., & Coblentz, D. (2004). Origin of the in situ stress field in south-eastern australia. *Basin Research*, *16*(3), 325–338.

Schellart, W. (2004). Quantifying the net slab pull force as a driving mechanism for plate tectonics. *Geophysical research letters*, *31*(7).

Stagpoole, V., & Nicol, A. (2008). Regional structure and kinematic history of a large subduction back thrust: Taranaki fault, new zealand. *Journal of Geophysical Research: Solid Earth*, *113*(B1).

Steinberger, B. (2000). Plumes in a convecting mantle: Models and observations for individual hotspots. *Journal of Geophysical Research: Solid Earth*, *105*(B5), 11127–11152.

Steinberger, B., Schmeling, H., & Marquart, G. (2001). Large-scale lithospheric stress field and topography induced by global mantle circulation. *Earth and Planetary Science Letters*, *186*(1), 75–91.

Stotz, I., Iaffaldano, G., & Davies, D. R. (2018). Pressure-driven poiseuille flow: a major component of the torque-balance governing pacific plate motion. *Geophysical Research Letters*, *45*(1), 117–125.

Sutherland, R. (1995). The australia-pacific boundary and cenozoic plate motions in the sw pacific: Some constraints from geosat data. *Tectonics*, *14*(4), 819–831.

Sutherland, R., Collot, J., Bache, F., Henrys, S., Barker, D., Browne, G., … others (2017). Widespread compression associated with eocene tonga-kermadec subduction initiation. *Geology*, *45*(4), 355–358.

Sutherland, R., Dickens, G. R., Blum, P., Agnini, C., Alegret, L., Asatryan, G., ... others (2020). Continental-scale geographic change across zealandia during paleogene subduction initiation. *Geology*, *48*(5), 419–424.

Torsvik, T. H., Müller, R. D., Van der Voo, R., Steinberger, B., & Gaina, C. (2008). Global plate motion frames: toward a unified model. *Reviews of geophysics*, *46*(3).

Wessel, P., & Kroenke, L. W. (2008). Pacific absolute plate motion since 145 ma: An assessment of the fixed hot spot hypothesis. *Journal of Geophysical Research: Solid Earth*, *113*(B6).

Whittaker, J., Muller, R., Leitchenkov, G., Stagg, H., Sdrolias, M., Gaina, C., & Goncharov, A. (2007). Major australian-antarctic plate reorganization at hawaiian-emperor bend time. *Science*, *318*(5847), 83–86.